Homogeneous swarm of high-Reynolds-number bubbles rising within a thin gap. Part 2. Liquid dynamics

Emmanuella Bouche, Véronique Roig, Frédéric Risso, Anne-Marie Billet

Homogeneous swarm of high-Reynolds-number bubbles rising within a thin gap. Part 2. Liquid dynamics

Emmanuella Bouche[1,3,‡], Véronique Roig[1,3,†], Frédéric Risso[1,3,†] and Anne-Marie Billet[2,3]

[1]Institut de Mécanique des Fluides de Toulouse, Université de Toulouse (INPT, UPS) and CNRS, Allée C. Soula, 31400 Toulouse, France

[2]Laboratoire de Génie Chimique, Université de Toulouse (INPT, UPS) and CNRS, 4 Allée E. Monso, BP 74233, 31432 Toulouse CEDEX 4, France

[3]Fédération de Recherche FERMaT, CNRS, Allée C. Soula, 31400 Toulouse, France

The agitation of the liquid phase has been investigated experimentally in a homogeneous swarm of bubbles rising at high Reynolds number within a thin gap. Owing to the wall friction, the bubble wakes are strongly attenuated. Consequently, liquid fluctuations result from disturbances localized near the bubbles and direct interactions between them. The signature of the average wake rapidly fades and the probability density function of the fluctuations becomes Gaussian as the gas volume fraction α increases. The energy of the fluctuations scales differently with α depending on the direction, indicating that hydrodynamic interactions are different in the horizontal and vertical directions. The spatial spectrum shows that the length scales of the fluctuations are independent of α and exhibits a k^{-3} subrange, which results from localized random flow disturbances of various sizes. Comparisons with the dynamics of the gas phase show that liquid and bubble agitations are driven by the same mechanism in the vertical direction, whereas they turn out to be almost uncoupled in the horizontal direction. Comparisons with unconfined flows show that the generation of liquid fluctuations is very different. However, the cause of the k^{-3} spectral subrange is the same for confined flows as for the spatial fluctuation of unconfined flows.

Key words: drops and bubbles, gas/liquid flow, multiphase and particle-laden flows

1. Introduction

In a previous companion paper (Bouche *et al.* 2012), we explored the dynamics of the gas phase in a homogeneous swarm of bubbles rising in a narrow cell in the inertial regime. In the present contribution, we focus on the dynamics of the liquid phase to achieve a complete description of the flow in a confined swarm.

We have already explored the agitation induced in the liquid phase by an isolated bubble rising in a Hele-Shaw cell at high Reynolds number (Roig *et al.* 2011). Owing

† Email addresses for correspondence: frederic.risso@imft.fr, veronique.roig@imft.fr

‡ Present address: CNRS, UMR 6614 CORIA, Université et INSA de Rouen, Avenue de l'Université, 76801 Saint Etienne du Rouvray, France.

to the confinement, the velocity perturbation induced in the liquid phase presents specific characteristics: (i) the velocity defect in the wake decreases exponentially, with a characteristic time scale controlled by the viscous diffusion across the gap of the cell, and (ii) two-dimensional vortices, which are released at the bubble rears, are damped before in-plane diffusion can affect them. The objective of the present paper is to give a comprehensive description of the agitation generated in the liquid phase by a confined swarm of rising bubbles and to evaluate the role of hydrodynamic interactions on this agitation.

This flow configuration is of interest for applications involving two-dimensional columns, such as those used in nuclear or spacecraft technology for cooling purposes (Spicka, Dias & Lopes 2001). Reliable predictions of the performances of these systems need careful investigations, as the confinement strongly affects the flow with respect to the reference case of a bubble swarm free to evolve in a three-dimensional space. In particular, the mixing of a high-Schmidt-number solute in a homogeneous swarm of bubbles rising in a Hele-Shaw cell was observed to be a non-Fickian process, contrary to what happens in unconfined flow (Bouche *et al.* 2013).

Moreover, this configuration is especially attractive for the fundamental understanding of the agitation induced by large-Reynolds-number rising bubbles. In an unconfined bubble swarm, the agitation has a dual nature (Risso *et al.* 2008) and combines two different contributions: the first, referred to as the spatial fluctuation, corresponds to the local spatial flow inhomogeneities in the vicinity of the bubbles; while the second, referred to as the temporal fluctuation, results from a collective instability of the bubble wakes, which produces turbulent fluctuations. Separating these two contributions is a hard task because the bubbles move. It is, however, possible by using both time and spatial averaging in a frame where the bubbles are at rest. This has been achieved experimentally by considering the flow crossing a random array of fixed spheres, which was proved to generate velocity fluctuations similar to those observed in a swarm of rising bubbles (Risso *et al.* 2010). It has also been done numerically from large-scale simulations of a homogeneous bubble swarm (Riboux, Legendre & Risso 2013). In the present configuration, the liquid agitation is generated by large-Reynolds-number rising bubbles with unstable wakes, while turbulence production is prevented by the strong confinement. Bubble-induced agitation in a confined cell thus involves a single contribution, which results from spatial flow inhomogeneities localized in the vicinity of the bubbles.

Fundamental issues are addressed from the present experimental investigation. We discuss how the properties of the bubble wakes and of their interactions determine the dynamics of the liquid agitation in confined and unconfined bubble swarms. We investigate the energy and the probability density functions (p.d.f.s) of the velocity fluctuations for various gas volume fractions α, with a particular focus on anisotropy and scaling laws. We also explore the spectra of the fluctuations and discuss them by considering the theoretical model of Risso (2011), which assumes uncorrelated velocity disturbances of random sizes and occurrences.

The paper is organized as follows. Section 2 describes the experimental set-up and the measuring methods. Section 3 successively presents and discusses the velocity perturbations around a test bubble, the statistics of the velocity fluctuations and the spatial spectra. Section 4 concludes with a synthesis of the main results.

2. Experimental set-up and instrumentation

2.1. *Description of the cell*

The experimental set-up is a Hele-Shaw cell consisting of two vertical glass plates of size 800 mm $\times$ 400 mm, separated by a gap of width $w = 1$ mm and filled with water

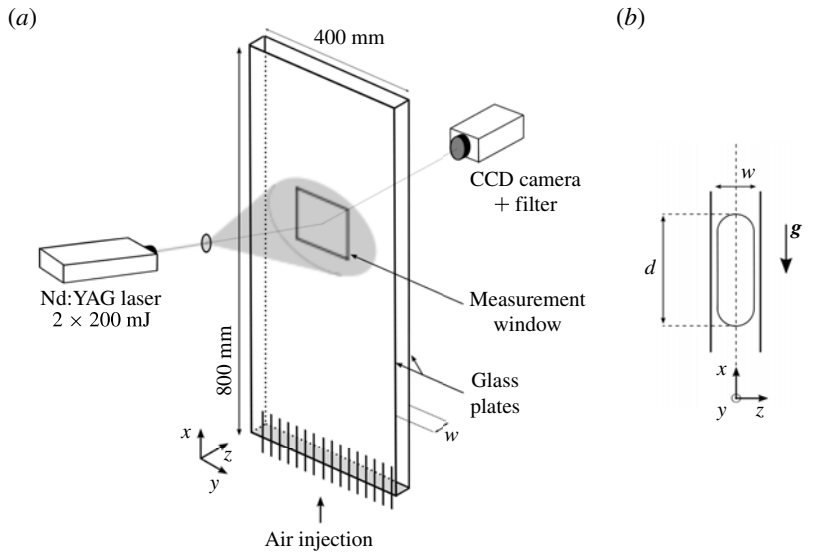

FIGURE 1. Schematic of the experimental set-up. (*a*) View of the cell, the CCD camera and the laser. (*b*) Side view of a bubble of equivalent diameter d confined within the gap of width w.

(Bouche *et al.* 2012). Bubbles are produced at the bottom of the cell by injection of air through a set of 16 capillary tubes (figure 1*a*). The gas volume fraction can be varied within the range $0.01 \leqslant \alpha \leqslant 0.12$, by adjusting the inlet air flow rate. A small amount of magnesium sulphate ($MgSO_4$) has been added to the water in order to prevent coalescence from occurring without significantly modifying either the density, the viscosity or the surface tension of water (Tsao & Koch 1994). The equivalent diameter of the bubbles is defined as $d = \sqrt{4A}/\pi$, where A is the bubble area projected onto the cell plane. The mean diameter varies from 3.9 to 4.6 mm as α increases and is large enough compared to the width w of the gap to ensure that the bubbles are strongly flattened due to the confinement (figure 1*b*).

The Archimedes number, $Ar = \sqrt{gd}\, d/\nu$, the Bond number, $Bo = \rho g d^2/\sigma$, and the confinement ratio, w/d, respectively, lie in the following ranges: $650 \leqslant Ar \leqslant 1100$, $1.7 \leqslant Bo \leqslant 3.5$ and $0.21 \leqslant w/d \leqslant 0.25$ (where g is the acceleration due to gravity, ρ is the water density, ν is its kinematic viscosity and σ is the surface tension). For such dimensionless groups, isolated bubbles rise at both large in-plane Reynolds number ($Re = V_0 d/\nu \approx 300$–$500$, where V_0 is the mean velocity of the bubble) and gap Reynolds number ($20 < Re(w/d)^2 < 24$), with constant elliptical in-plane shapes (aspect ratio ≈ 1.3) and unstable wakes with periodic vortex shedding (Roig *et al.* 2011).

In the region of investigation, far enough from the injection, the profiles of the gas volume fraction and of the bubble velocities were proved to be uniform, showing that the flow in the swarm is homogeneous (Bouche *et al.* 2012).

2.2. *Velocity measurements*

The liquid velocity within the gap is parallel to the cell walls, except in the close vicinity of the bubbles. We therefore describe the liquid motion by the velocity averaged over the gap: $\boldsymbol{u}(x, y, t) = u_x \boldsymbol{e}_x + u_y \boldsymbol{e}_y$. It is measured by means of particle

image velocimetry (PIV) with volume lighting, a particular technique described in Roudet *et al.* (2011). This velocity proved to be relevant to analyse the coupling between the dynamics of a single bubble and its wake (Roig *et al.* 2011). For the present study, the two-dimensional velocity field $\boldsymbol{u}(x, y, t)$ provides a rather complete description of the liquid motion in a bubble swarm, except in the close vicinity of the bubbles. One advantage of confined bubbly flows is that there is no bubble overlapping. Bubble contours are therefore easily detected on each image (Bouche *et al.* 2012). The volume fraction is accurately determined from the ratio of the area occupied by the bubbles to the total flow area. Furthermore, the liquid velocity is measured without the need for complex phase discrimination.

PIV is performed using a Nd:YAG pulsed laser (Quantel Multipulse, two $\times$200 mJ, $\lambda = 532$ nm) and a charge-coupled device (CCD) camera (PCO, 1376 pixel $\times$ 1024 pixel) equipped with a lens of 85 mm focal length. A high-pass optical filter with a cut-off wavelength of 580 nm is fixed on the lens in order to filter the incident laser light. The optical axes of the camera and the incident laser beam are both horizontal, but while the camera is perpendicular to the cell, the laser is set at an angle of 30° to avoid direct illumination of the CCD (figure 1*a*). Poly(methyl methacrylate)-encapsulated particles of rhodamine B of 10–20 μm are added to the aqueous solution to serve as fluorescent tracers. The camera depth of field is larger than the width of the gap, and an array of spherical micro-lenses make the laser beam diverge, providing volume illumination of the cell (figure 1*a*). The measurement window is a rectangle of size 120 mm $\times$ 90 mm, the centre of which is located 360 mm above the capillary tubes and at the middle of the cell in the horizontal direction (figure 1*a*). It is divided into PIV interrogation cells of 16 pixel $\times$ 16 pixel with an overlap of 50 %, resulting in a spatial resolution of 1.45 mm.

The velocity field is calculated from pairs of images separated by $\Delta t = 3$ ms. The sampling frequency, $f = 1$ Hz, is low enough to ensure that successive velocity fields are uncorrelated, which ensures a rapid statistical convergence of the p.d.f.s. The calculation is done by means of a home-made PIV software (PIVis) based on an iterative multi-pass algorithm. In order to obtain relevant PIV measurements, the number of tracers in an interrogation cell must be larger than $\simeq$ 10–15 (Adrian 1991). This leads to an additional experimental difficulty coming from the depletion of the tracers, which are captured by the bubble interfaces and progressively brought to the free surface at the top of the cell. This process, which is enhanced as the gas volume fraction increases, does not allow the recording of long time series. A preliminary test was performed to determine the optimal recording duration. For each gas volume fraction, velocity fields are computed every second during 500 s. The quality of the PIV calculations is then assessed from the examination of the average signal-to-noise ratio, the width and the amplitude of the intercorrelation peak, as well as the occurrence of peak locking. It turned out that the maximum duration allowing reliable and accurate measurements was between 60 and 100 s, depending on α.

After running the PIV algorithm, two-dimensional velocity fields show spurious vectors, which are detected by means of the method based on the normalized median residual introduced by Westerweel & Scarano (2005). The proportion of spurious vectors increases with the gas volume fractions: it was 2.8 % at $\alpha = 1.2$ % and 25 % at $\alpha = 12$ %. However, most of them are located in the immediate vicinity of bubbles, within interrogation cells that are either crossed by a portion of a gas–liquid interface (where trapped rhodamine tracers accumulate) or dazzled by the light reflected by a close interface. We therefore removed all measurements obtained at less than 3–4 interrogation cells from a gas–liquid interface. After this operation, the number

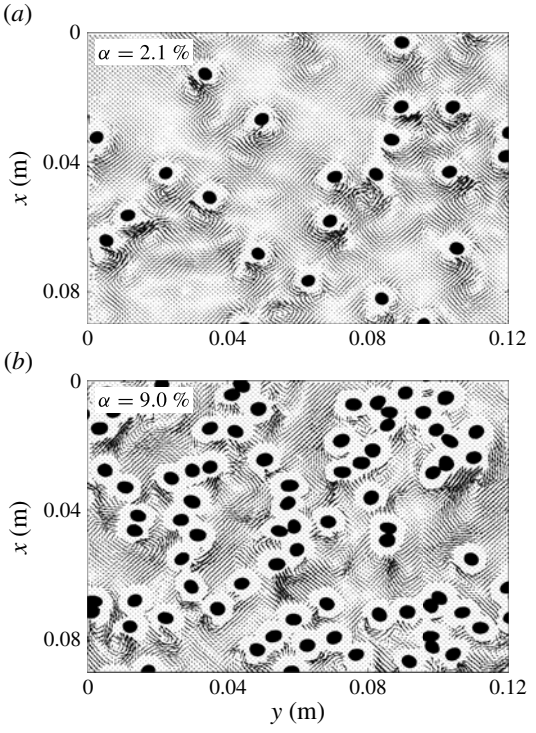

FIGURE 2. Two-dimensional velocity fields for (*a*) $\alpha = 2.1\,\%$ and (*b*) $\alpha = 9\,\%$. Bubbles are marked in black; regions near the bubble interfaces where the velocity is not measured are empty of vectors.

of spurious vectors becomes insignificant at low α and remains less than $5\,\%$ in the worst case at the largest volume fraction. The few remaining spurious vectors detected outside the vicinity of any bubble have been removed and replaced by interpolating correct vectors by using the MATLAB function 'griddata', which is based on Delaunay's triangulation.

Statistical quantities of the liquid velocity (average, variance and spectrum) are calculated from at least 120 PIV fields, so that statistical convergence is ensured.

3. Results and discussion

Figure 2(*a*,*b*) shows instantaneous velocity fields for two gas volume fractions ($\alpha = 2.1\,\%$ and $9\,\%$). At low volume fraction (figure 2*a*), it is clearly seen that bubble-induced perturbations are localized close to the bubbles: vortices generated at the bubble rears are clearly identifiable in short von Kármán streets, and regions distant from any bubble are at rest. When the gas volume fraction is increased (figure 2*b*), the bubbles become closer to each other and the flow perturbations they induce combine themselves. It becomes less easy to detect motionless regions or to identify the wake associated with a given bubble. In addition, unsteady velocity perturbations of various sizes are present in the flow.

The velocity disturbances generated by the bubbles are the cause of the liquid agitation. Before considering the statistics of the liquid agitation, it is therefore relevant to start by considering the average flow around a bubble inside the bubble

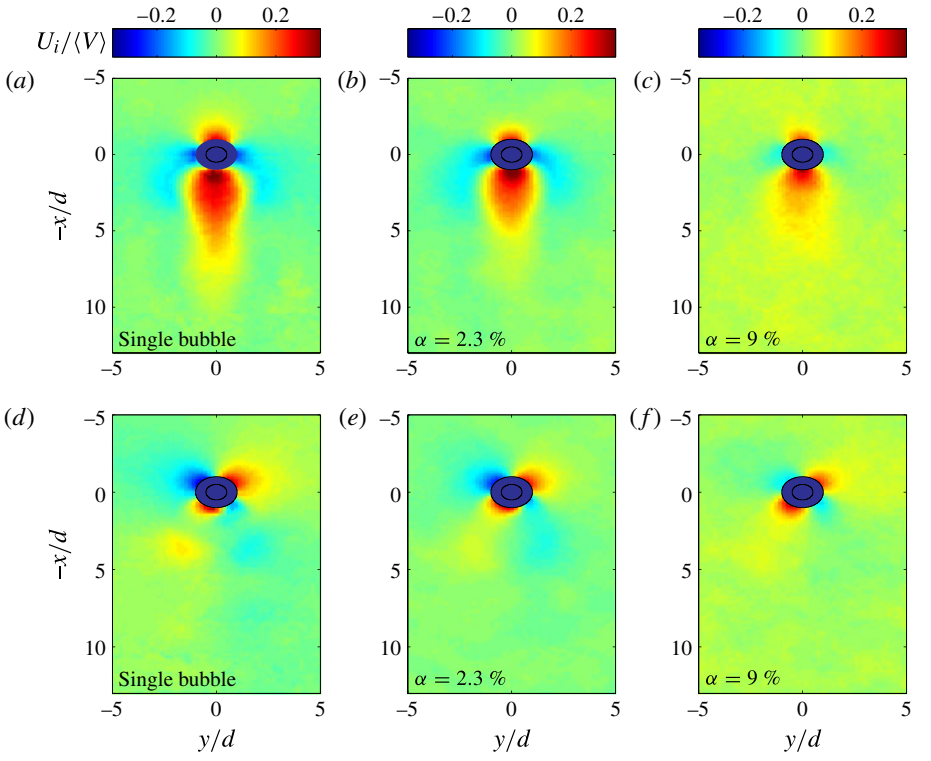

FIGURE 3. (Colour online) Average liquid velocity field around a bubble within the swarm: (*a–c*) vertical velocity U_x; (*d–f*) horizontal velocity U_y; for (*a*,*d*) isolated bubble ($\alpha = 0$), (*b*,*e*) $\alpha = 2.1\,\%$ and (*c*,*f*) $\alpha = 9\,\%$. The bubble contour at an instant when its axis is vertical is marked by a black line. No measurement is available in the close vicinity of the bubble, which is dark coloured (blue online). In print in grey levels, the scale represents the absolute value of the velocity components, $|U_x|$ and $|U_y|$. Viewed online in colour, the scale represents the signed values, U_x and U_y.

swarm. The way this flow depends on the gas volume fraction should shed light on hydrodynamic interactions.

3.1. *Average liquid flow around a bubble*

The average velocity perturbation $\boldsymbol{U}(x, y)$ around a bubble inside the swarm has been determined from PIV measurements. It has been calculated as the average of the liquid velocity conditioned by the location of the considered point relatively to each bubble centre. Figure 3 shows the fields of the vertical and horizontal average perturbations, U_x and U_y, normalized by the average bubble velocity $\langle V\rangle$, for $\alpha = 2.1\,\%$ and $9\,\%$. These velocity fields are very similar to the average velocity of a bubble conditioned by the presence of another bubble located at the origin (see figure 7 of Bouche *et al.* (2012)), which confirms the dominant role of the entrainment by the wakes in the dynamics of the gas phase. The vertical perturbation U_x has larger intensity and spatial extension than U_y, indicating the significant contribution of an average quasi-parallel wake. However, for both directions, these results confirm the small spatial extension of the average perturbation, which remains confined in the close vicinity of the bubble. In

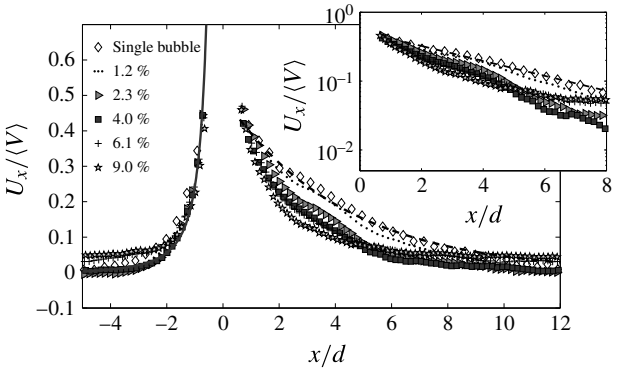

FIGURE 4. Average of the liquid vertical velocity U_x along the vertical axis passing through the bubble centre, normalized by the average bubble velocity $\langle V\rangle$, for various gas volume fractions. Solid line: potential solution above the bubble. Dashed line: $\exp(-x/4.2d)$, exponential fit of the experimental results obtained for an isolated bubble from Roig *et al.* (2011). The inset displays a semi-logarithmic plot of the wake with the aim to show the exponential decay.

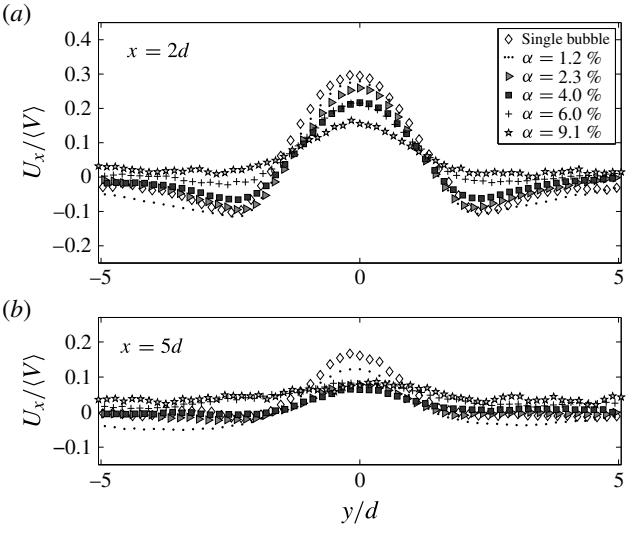

FIGURE 5. Horizontal profiles of the average vertical liquid velocity U_x normalized by the average bubble velocity $\langle V\rangle$, at (*a*) $2d$ and (*b*) $5d$ below the bubble centre, for various gas volume fractions.

order to quantify the decay of the wake, figure 4 shows the evolution of U_x along the vertical axis passing through the bubble centre, while figure 5 shows the horizontal profiles of U_x at respectively $2d$ and $5d$ behind the bubble centre, for various gas volume fractions.

At low gas volume fraction ($\alpha \leqslant 1.2\,\%$), bubble interactions have a weak influence and the average perturbation induced by a bubble inside the swarm is almost the same as that of an isolated bubble, which has been described in detail by Roig *et al.* (2011). Above the bubble, the average flow perturbation is potential. Behind the bubble, the

wake decays exponentially as $U_x/\langle V\rangle \approx \exp(-x/l_v)$ (figure 4), where the length scale $l_v = 4.2d$ is fixed by the wall friction and can be expressed as a function of the viscous length scale as $l_v = \langle V\rangle w^2/(6.7\nu)$. It is worth noting that, while the wake decays very quickly, the width of the wake does not significantly evolve with the distance to the bubble (figure 5). This confirms that momentum diffusion in the plane of the cell is negligible, the wake decay being controlled by the friction on the cell walls.

As the gas volume fraction is increased, the average perturbation above the bubble is weakly influenced by the presence of the other bubbles and remains potential. On the other hand, the decay of the average wake is enhanced by the perturbations induced by the neighbouring bubbles. It remains exponential, with a length scale that first decreases as α increases, and eventually reaches a constant value for $\alpha \gtrsim 2\,\%$ (figure 4). For $\alpha \geqslant 4\,\%$, the average perturbation can be considered as negligible from a distance of $5d$ behind a bubble.

The flow perturbation around a bubble inside a three-dimensional unconfined swarm has been described by Risso & Ellingsen (2002), Roig & Larue de Tournemine (2007) and Risso *et al.* (2008). Surprisingly, it shares the same characteristics as the present average flow measured around a bubble in a confined swarm: potential flow above the bubble and exponentially decaying wake behind. Moreover, the length scale of the exponential decays is observed in both cases to become almost independent of the gas volume fraction beyond a certain value of α. Nevertheless, the physical mechanisms responsible for the wake attenuation are totally different. In a three-dimensional bubble swarm, the wake attenuation is caused by wake interactions that start to become significant from a volume fraction of approximately 0.5 %. In a two-dimensional bubble swarm, it is caused by the friction at the cell walls.

Even if the hydrodynamics of confined and unconfined flows are of a different nature, we may expect that the statistical properties of the liquid agitation in a two-dimensional bubble swarm may share some properties with that of the spatial fluctuation in a three-dimensional bubble swarm. This now needs to be checked, since the average perturbation of the flow around a bubble does not account for the contributions of the unsteady vortices that are released at the bubble rears.

3.2. *Statistics of the velocity fluctuations*

Figure 6 shows the standard deviations of the two liquid velocity components as a function of the gas volume fraction. For $\alpha = 1\,\%$, the two fluctuations have similar intensity. Then, the vertical fluctuation $\langle u_x^2\rangle^{1/2}$ increases as $\alpha^{0.46}$, while the horizontal fluctuation $\langle u_y^2\rangle^{1/2}$ increases as $\alpha^{0.38}$, which leads to an increasing predominance of the vertical fluctuation. In the absence of hydrodynamic interactions between the flows induced by each bubble, the fluctuating energy is expected to be proportional to the volume fraction, and the standard deviations should therefore scale as $\alpha^{1/2}$. The deviation of the exponents relative to 1/2 is hence a signature of hydrodynamic interactions. Here, the fact that two different exponents are observed indicates that hydrodynamic interactions have different effects in the two directions. It is reasonable to think that the combination of the wakes of the bubbles that are close to each other are more efficient in enhancing vertical fluctuations.

Figure 7 presents p.d.f.s of the fluctuations for various gas volume fractions. In panels (*a*) and (*b*), a linear scale is used and the fluctuations are normalized by the velocity V_0 of an isolated bubble rising within the cell. As expected, the p.d.f.s broaden as α is increased. The horizontal p.d.f.s are symmetric whereas the presence of the wakes behind the bubbles makes the vertical p.d.f.s asymmetric, with large

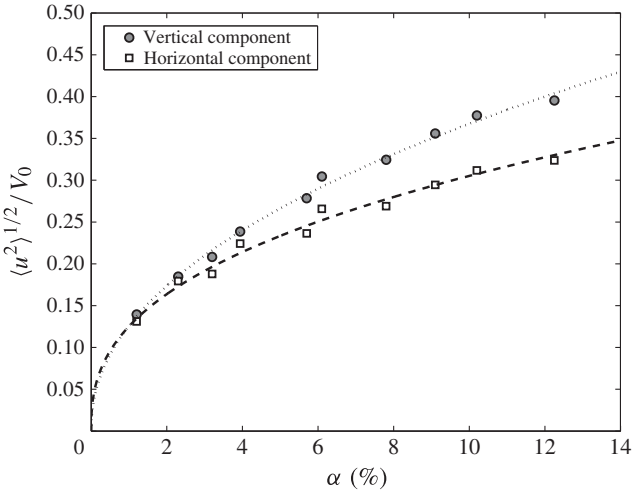

FIGURE 6. Standard deviations of the liquid vertical and horizontal velocities normalized by the rising velocity of an isolated bubble V_0, as a function of the gas volume fraction α. Dotted line: fit of the vertical component, $1.07\alpha^{0.46}$. Dashed line: fit of the horizontal component, $0.74\alpha^{0.38}$.

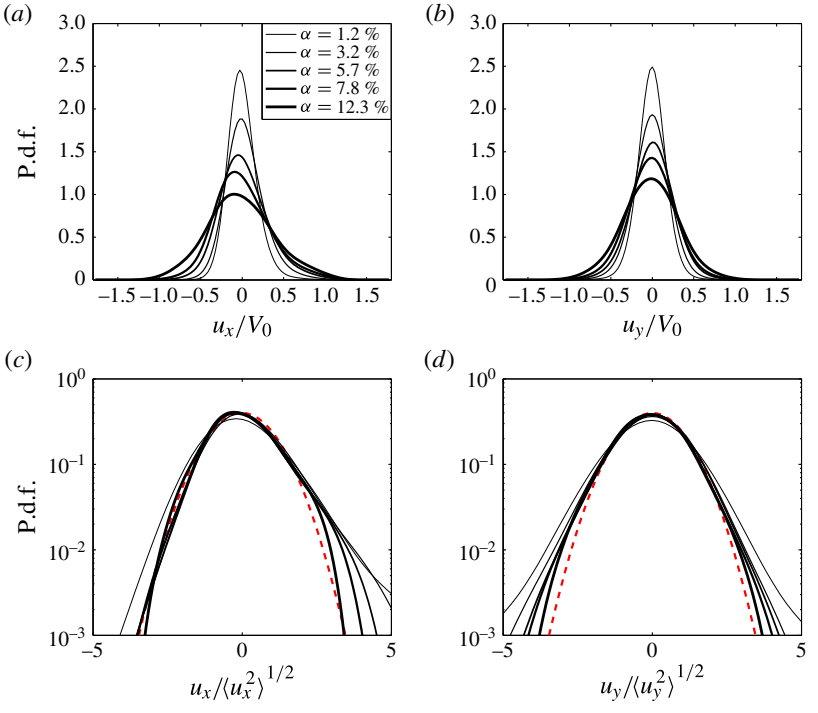

FIGURE 7. Probability density functions of liquid velocity fluctuations for various gas volume fractions. (*a*) Vertical fluctuation normalized by the rising velocity of an isolated bubble (linear plot). (*b*) Horizontal fluctuation normalized by the rising velocity of an isolated bubble (linear plot). (*c*) Vertical fluctuation normalized by the standard deviation (semi-logarithmic plot). (*d*) Horizontal fluctuation normalized by the standard deviation (semi-logarithmic plot). The dashed lines show the Gaussian distribution with the same variance.

fluctuations that are more probable in the upward direction. In panels (*c*) and (*d*), a semi-logarithmic representation is used and the fluctuations are normalized by their standard deviation. At $\alpha = 1.2\,\%$, the departure from a Gaussian distribution of the same standard deviation is significant. Then, as α increases, the p.d.f.s converge towards a Gaussian distribution. At $\alpha = 12\,\%$, even the signature of the bubble wakes in the p.d.f. of the vertical fluctuations, which is characterized by a tail for large positive values of u_x, has almost disappeared.

It is interesting to compare the statistics of the liquid velocity to those of the bubble velocity, which have been described in Bouche *et al.* (2012). In the vertical direction, bubble fluctuations show the same trends as liquid fluctuations: their standard deviation also scales as $\alpha^{0.46}$; their p.d.f.s exhibit similar asymmetric shapes at low α that converge towards a Gaussian distribution when α is increased. This suggests that bubble and liquid vertical fluctuations result from the same physical mechanism. On the contrary, in the horizontal direction, bubble and liquid fluctuations manifest totally different trends. Bubble fluctuations are driven by wake instabilities that generate bubble path oscillations. Consequently, their standard deviation turns out to be independent of α, while their p.d.f.s distinctly show the signature of these oscillations. Since the intensity of horizontal liquid fluctuations instead regularly increases with α, bubble and liquid fluctuations turn out to be uncoupled in the horizontal direction.

Let us now compare the present results to the liquid fluctuations that are observed in an unconfined bubble swarm for a similar flow regime. Experimental measurements obtained in a three-dimensional homogeneous bubble swarm (Riboux, Risso & Legendre 2010) show different features compared to two-dimensional bubble swarms. Vertical and horizontal fluctuations both scale as $\alpha^{0.4}$, which implies that the level of anisotropy remains constant as α increases. The p.d.f.s are independent of α when normalized using the standard deviation and show an exponential decay as u_x or u_y increases. Moreover, the signature of the wake does not disappear and the p.d.f.s do not tend towards a Gaussian distribution. The results of large-scale simulations (Riboux *et al.* 2013) show that both the spatial and temporal contributions to the fluctuations adopt exponential self-similar p.d.f.s. In addition, neither the standard deviations of the spatial fluctuations, nor that of the temporal ones, show a scaling with α that corresponds to what is observed in the confined bubble swarm. Even if exponentially attenuated wakes are observed in both confined and unconfined flows, the statistics of the velocity fluctuations do not have the same characteristics. In three-dimensional bubble swarms, the major mechanism is the development of a collective instability of the flow generated by all the bubbles. In two-dimensional bubble swarms, the confinement constrains hydrodynamic perturbations to remain localized in the vicinity of the bubbles. The major mechanism corresponds therefore to one-to-one interactions between bubbles. Since these interactions are not the same in the vertical and horizontal directions, the scaling of the fluctuations with α depends on the direction. Moreover, these interactions are very efficient in attenuating the steady part of an individual wake, which causes the signature of the wakes to vanish and the p.d.f.s to converge towards a Gaussian distribution.

3.3. *Spatial spectra of the fluctuations*

In unconfined bubbly flows, liquid fluctuations are known to present particular features (Lance & Bataille 1991; Resen, Luther & Lohse 2005; Martinez Mercado *et al.* 2010; Riboux *et al.* 2010; Mendez-Diaz, Serrano-García & Zenit 2013). In the absence of

shear-induced turbulence, a k^{-3} subrange is always observed in the spectra. Riboux *et al.* (2013) showed that both the spatial and temporal fluctuations exhibit such a spectral behaviour, which implies that a k^{-3} subrange should be observed whether fluctuations are dominated by the flow disturbances generated by individual bubbles or by real bubble-induced turbulence. It is therefore interesting to consider the spectra in a confined bubbly flow, where liquid fluctuations are only due to flow disturbances in the vicinity of the bubbles.

The determination of spectra in bubbly flows is complicated by the fact that velocity signals are interrupted by the passage of the bubbles. As reported in the literature, different methods have been used to deal with this difficulty, such as smoothing the discontinuities by a Gauss function (Lance & Bataille 1991), considering only intervals between bubbles where the signal is continuous (Martinez Mercado *et al.* 2010), and investigating the flow behind a rising swarm of bubbles (Riboux *et al.* 2010).

Here, we have chosen to use a method similar to that of Martinez Mercado *et al.* (2010). We consider each uninterrupted piece of length l of the one-dimensional signals along the columns (vertical direction) or the rows (horizontal direction) of the PIV velocity field. Then, we compute the average spectrum, S_{xx}, of the vertical velocity along the vertical direction and the average spectrum, S_{yy}, of the horizontal velocity along the horizontal direction. The choice of l results from a compromise. If chosen too short, significant large scales are not described. If chosen too long, the number a samples is too small to ensure statistical convergence. The value of l that has been chosen corresponds to the maximum value ensuring that the variance of the fluctuations computed on the retained velocity samples matches the value computed over all measurements. Depending on the direction and on the gas volume fraction, the optimal values of l varied between 72 and 121 mm. Owing to the spatial resolution of the PIV, the present method thus allows the description of length scales ranging between 2.9 and $\sim$100 mm.

Figure 8 shows the vertical and horizontal spectra as a function of the reciprocal of the wavelength, $\lambda^{-1} = k/2\pi$, for various gas volume fractions. Comparably to what is observed for the p.d.f.s, the spectra of the vertical and horizontal fluctuations are quite similar. Provided they are normalized by the variance of the corresponding fluctuations, all horizontal spectra (vertical spectra) collapse onto a single curve, indicating that the length scales of the velocity fluctuations do not depend on α – a property already observed for the large scales in unconfined bubbly flows. The Eulerian integral length scale (estimated from the extrapolation of the normalized spectrum at wavenumbers tending to zero) is close to 20 mm. A power-law evolution as λ^3 is observed in the range from $\lambda_{min} \sim 5$ to $\lambda_{max} \sim 20$ mm, in both vertical and horizontal spectra.

A theoretical model has been developed by Risso (2011) for the spectrum of the spatial contribution to the bubble-induced agitation. Bubbles are assumed to generate localized random velocity disturbances, which have the following elementary properties: they have a smooth and regular pattern, they are uniformly distributed over space, their strength and size are statistically independent, and their size is uniformly distributed between two finite lengths λ_{min} and λ_{max}. Under these assumptions, it is demonstrated that the spectrum evolves as λ^3 between λ_{min} and λ_{max}.

Here, the fluctuations generated by the bubbles result from both (i) the average velocity disturbance, which has been described in § 3.1, and (ii) the unsteady vortices that are released from the bubble rears. Since the locations of the bubbles have been proved to be independent of each other (Bouche *et al.* 2012), the disturbances they generate can be assumed to be uniformly distributed over space. In addition, the fact that the p.d.f.s tend towards a Gaussian distribution as α increases suggests that

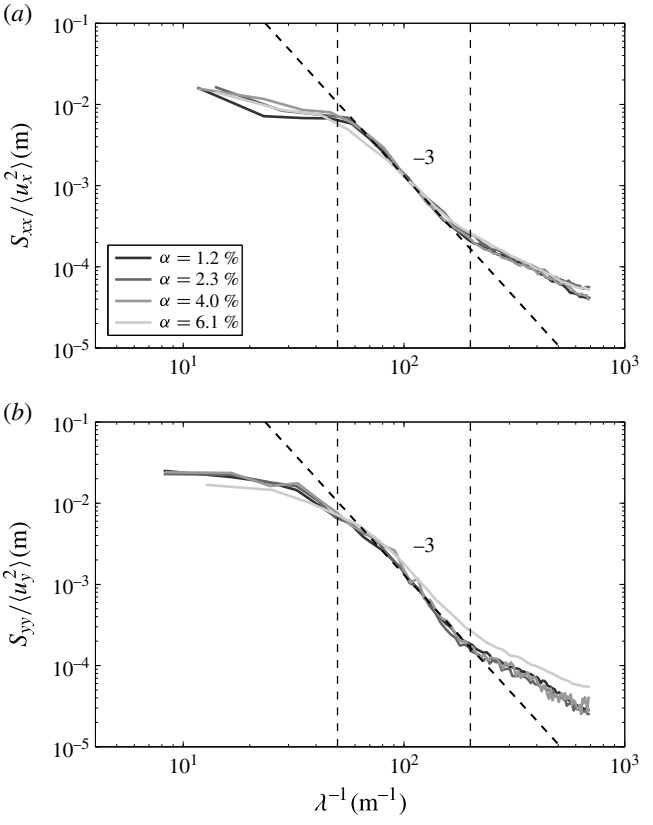

FIGURE 8. Normalized longitudinal spatial spectra of the liquid velocity fluctuations, for various gas volume fractions: (*a*) vertical spectra S_{xx}; (*b*) horizontal spectra, S_{yy}.

fluctuations result from the addition of independent stochastic events. Moreover, the flow structures visible in the instantaneous velocity fields (figure 2) have dimensions that range between approximately d (∼4–5 mm) and the length of the average wake, $5d$ (∼20 mm), which approximately correspond to the values of λ_{min} and λ_{max} obtained from the measured spectra.

Confined bubbly flows thus seem to ideally fit in the domain of validity of the model, and the explanation of the existence of a λ^3 range is similar to that of the spatial fluctuations in unconfined flows.

4. Conclusion

Owing to the confinement, neither turbulence nor a collective instability involving distant wakes can develop. Liquid velocity fluctuations in a Hele-Shaw cell mainly result from velocity disturbances localized near the bubbles and direct interactions between them. These disturbances include the contributions of the average wakes and of unsteady vortices that are generated at the bubble rears. The wakes are strongly attenuated by wall friction, so they decay exponentially and have almost vanished at a distance of $5d$ behind a bubble. The energy of the fluctuations increases with the gas volume fraction, but the evolution of the standard deviation differs depending on the direction: it scales as $\alpha^{0.46}$ in the vertical direction, whereas it scales as $\alpha^{0.38}$ in the

horizontal direction. Hydrodynamic interactions therefore do not have the same effect in both directions. As the gas volume fraction increases, the relative contribution of the average wakes decreases and the p.d.f.s of the fluctuations tend towards a Gaussian distribution. Provided they are normalized by the variance of the fluctuations, spatial spectra turn out to be independent of α, with an integral length scale close to the wake length. Moreover, the power spectral density is observed to evolve as k^{-3} in the range from $\lambda_{min} \sim 5$ to $\lambda_{max} \sim 20$ mm.

The dynamics of vertical liquid fluctuations shows characteristics similar to that of the vertical bubble fluctuations: same scaling of the energy with α, similar p.d.f.s, and an integral scale that is imposed by the wake length and that does not depend on α. In the vertical direction, bubble and liquid agitations are hence controlled by the same physical mechanism. In the horizontal direction, the properties of the two phases are instead totally different; the liquid agitation is almost uncoupled from the bubble dynamics, which is driven by bubble path oscillations induced by wake instabilities.

In an unconfined bubbly flow, two causes of fluctuations are present: (i) flow disturbances that are localized in the bubble vicinity, and (ii) a collective instability that involves all the bubble wakes and generates the development of turbulence. In a confined flow, only the first source of agitation is present. The comparison between confined and unconfined bubbly flows is therefore particularly useful to understand the physical mechanisms responsible for the singular properties of the bubble-induced agitation. Surprisingly, average wakes are observed to decay exponentially in both two- and three-dimensional cases. However, this a coincidence since the causes of the wake attenuation are of different natures: wall friction in confined flows and interactions with neighbouring wakes in unconfined flows. The statistics of the liquid velocity fluctuations show different properties in unconfined flows: the standard deviation of the fluctuations scales as $\alpha^{0.4}$ and does not depend on the direction; the signature of the wake remains clearly visible in the p.d.f.s (of both temporal and spatial contributions), which keep an exponential decay as α increases. On the other hand, the spectra share the same main characteristics: independence of the large scales with the gas volume fraction, with an integral scale that corresponds to the wake length, and the existence of a k^{-3} subrange. Interestingly, the cause of the existence of a k^{-3} subrange is the same for confined flows as for the spatial fluctuation of unconfined flows (Risso 2011). It results from localized random flow disturbances of various sizes.

REFERENCES

ADRIAN, R. J. 1991 Particle imaging techniques for experimental fluid mechanics. *Annu. Rev. Fluid Mech.* **23**, 261–304.

BOUCHE, E., CAZIN, S., ROIG, V. & RISSO, F. 2013 Mixing in a swarm of bubbles rising in a confined cell measured by mean of PLIF with two different dyes. *Exp. Fluids* **54**, 1552.

BOUCHE, E., ROIG, V., RISSO, F. & BILLET, A. M. 2012 Homogeneous swarm of high-Reynolds-number bubbles rising within a thin gap. Part 1. Bubble dynamics. *J. Fluid Mech.* **704**, 211–231.

LANCE, M. & BATAILLE, J. 1991 Turbulence in the liquid phase of a uniform bubbly air–water flow. *J. Fluid Mech.* **222**, 95–118.

MARTINEZ MERCADO, J., CHEHATA GOMEZ, D., VAN GILS, D., SUN, C. & LOHSE, D. 2010 On bubble clustering and energy spectra in pseudo-turbulence. *J. Fluid Mech.* **650**, 287–306.

MENDEZ-DIAZ, S., SERRANO-GARCÍA, J. C. & ZENIT, R. 2013 Power spectral distributions of pseudo-turbulent bubbly flows. *Phys. Fluids* **25**, 043303.

RESEN, J., LUTHER, S. & LOHSE, D. 2005 The effect of bubbles on developed turbulence. *J. Fluid Mech.* **538**, 153–187.

RIBOUX, G., LEGENDRE, D. & RISSO, F. 2013 A model of bubble-induced turbulence based on large-scale wake interactions. *J. Fluid Mech.* **719**, 362–387.

RIBOUX, G., RISSO, F. & LEGENDRE, D. 2010 Experimental characterization of the agitation generated by bubbles rising at high Reynolds number. *J. Fluid Mech.* **643**, 509–559.

RISSO, F. 2011 Theoretical model for k^{-3} spectra in dispersed multiphase flows. *Phys. Fluids* **23**, 011701.

RISSO, F. & ELLINGSEN, K. 2002 Velocity fluctuations in a homogeneous dilute dispersion of high-Reynolds-number rising bubbles. *J. Fluid Mech.* **453**, 395–410.

RISSO, F., ROIG, V., AMOURA, Z. & BILLET, A.-M. 2010 The dual nature of pseudo-turbulence analyzed from spatial and time averagings of a flow through random obstacles. In *Proceedings of the 7th International Conference on Multiphase Flows (ICMF) 2010, Tampa, FL, 30 May–4 June*.

RISSO, F., ROIG, V., AMOURA, Z., RIBOUX, G. & BILLET, A.-M. 2008 Wake attenuation in large Reynolds number dispersed two-phase flows. *Phil. Trans. R. Soc. Lond.* A **366**, 2177–2190.

ROIG, V. & LARUE DE TOURNEMINE, A. 2007 Measurement of interstitial velocity of homogeneous bubble flows at low to moderate void fraction. *J. Fluid Mech.* **572**, 87–110.

ROIG, V., ROUDET, M., RISSO, F. & BILLET, A.-M. 2011 Dynamics of a high-Reynolds-number bubble rising within a thin gap. *J. Fluid Mech.* **707**, 444–466.

ROUDET, M., BILLET, A.-M., RISSO, F. & ROIG, V. 2011 PIV with volume lighting in a narrow cell: an efficient method to measure large velocity fields of rapidly varying flows. *Exp. Therm. Fluid Sci.* **35**, 1030–1037.

SPICKA, P., DIAS, M. M. & LOPES, J. C. B. 2001 Gas–liquid flow in a 2D column: comparison between experimental data and CFD modelling. *Chem. Engng Sci.* **56**, 6367–6383.

TSAO, H.-K. & KOCH, D. L. 1994 Collisions of slightly deformable, high Reynolds number bubbles with short-range repulsive forces. *Phys. Fluids* **6**, 2591–2625.

WESTERWEEL, J. & SCARANO, F. 2005 Universal outlier detection for PIV data. *Exp. Fluids* **39**, 1096–1100.